Mon. Not. R. Astron. Soc. **284,** 541–551 (1997)

A study of cores in a complete sample of radio sources

R. Morganti,[1,2] T. A. Oosterloo,[2] J. E. Reynolds,[2] C. N. Tadhunter[3] and V. Migenes[2]

[1]*Istituto di Radioastronomia, CNR, via Gobetti 101, I-40129 Bologna, Italy*
[2]*Australia Telescope National Facility, CSIRO, PO Box 76, Epping, NSW 2121, Australia*
[3]*Department of Physics, University of Sheffield, Sheffield S3 7RH*

Accepted 1996 August 19. Received 1996 February 22

ABSTRACT

The high resolution provided by the Parkes–Tidbinbilla real-time interferometer (PTI) has been used to measure the core flux density for a complete sample of radio sources. Lower resolution maps are already available for most of these objects together with optical (spectroscopic) data. The new data show that an inverted spectral index $\alpha \sim -0.3$ ($S \propto \nu^{-\alpha}$) could be characteristic of *all* the nuclei, going from low-luminosity radio galaxies to powerful quasars. Taking this spectral index into account, the measured flux density does not change very much, going from a scale of tens of kpc (corresponding to the low-resolution observations) to the sub-kpc scale of the new observations. Thus, most of the flux observed in the central region originates in a sub-kpc area.

With the new PTI data we obtain a better estimate of the radio core dominance (R), i.e. the ratio between the core and the extended radio flux. This parameter is claimed to be a good indicator of the orientation of the beamed radiation with respect to the line of sight, and hence a very important parameter for testing 'unified schemes' for active galactic nuclei (AGN). Using this parameter, together with optical spectroscopic information, we find that the radio core dominance shows different distributions for different radio and optical characteristics. A statistically significant difference in the distribution of R is observed between Fanaroff–Riley (FR) I and FR II radio galaxies, supporting the idea that low-power sources are less affected by beaming because they have, on average, a lower Lorentz factor. Among the FR II radio galaxies, narrow-line radio galaxies (NLRGs) show lower values of R while the broad-line radio galaxies (BLRGs) have the largest R. Moreover, the median value of R for BLRGs is lower than for steep-spectrum quasars (SSQ) even after a number of selection effects are taken into account. This result can be explained in the framework of unified schemes for AGN assuming that in the BLRGs we are seeing more directly into the nucleus, although not as much as in SSQs.

Key words: galaxies: active – radio continuum: general.

1 INTRODUCTION

The central region of a radio source is believed to contain the 'engine', in which the energy to fuel the extended structure (large-scale emission) is produced. Although extremely interesting, the study of this region is obviously complicated by the resolution required for the observations. If we consider, as the nucleus of a radio source, the compact region observed on the very long baseline interferometry (VLBI) scale (i.e. parsec scale, although the region characteristic of the optical broad-line emission is likely to be smaller), every radio observation with lower resolution will then include part of the emission outside the nucleus, and the definition of 'core' becomes uncertain. In particular, when studied using VLBI techniques, the nuclear region usually (although more and more exceptions are being found, see

Readhead 1993) shows an asymmetric jet emerging from a compact nucleus. The asymmetry observed in the jets is commonly attributed to the bulk relativistic motion of the plasma in the jet and the consequent beaming of the emission in the forward direction. Observations of the nuclear region with resolution lower than the typical VLBI are likely to include, in what we will be calling the 'core', the beginning of the jet, i.e. part of the beamed emission.

Beaming and orientation effects also play an important role at wavelengths different from the radio. At optical wavelengths, orientation effects in the emission from the central region are believed to be produced by obscuration because of the presence of a thick disc or torus. For example, in the unified scheme proposed by Barthel (1989), the differences between narrow and broad-line radio galaxies and quasars are believed to be the result of obscuration effects, the latter having the *UV* emission from the nucleus more aligned with the line of sight and allowing the observer to look more deeply into the AGN.

A beamed component is likely to be present also in the X-ray and γ-ray emission, at least in quasars (Wilkes 1994 and references therein) and possibly also in some radio galaxies (Fabbiano et al. 1984; Siebert et al. 1996).

Thus, if beaming and orientation effects are so important, the nuclear radio emission and the characteristics at other wavelengths of the nuclear emission should show some kind of relationship. The core dominance [i.e. $R=S_{\rm core}/(S_{\rm tot}-S_{\rm core})$; Orr & Browne 1982] is considered the best indicator of the orientation of the beamed radiation with respect to the line of sight; objects for which R is large are more likely to have their beamed radiation emitted in a direction close to the line of sight. The R parameter can therefore be used to test some of the predictions made by the unified schemes. For example, we can test whether broad-line radio galaxies (BLRGs) can be considered as an intermediate group between narrow-line radio galaxies (NLRGs) and quasars, or if they are the low-redshift equivalent of quasars (QSRs). A trend between the value of R and the width of the optical emission lines has been reported by Hine & Longair (1979) for a sub-sample of the 3CR sample of radio sources. On the other hand, evidence has been reported by Morganti, Killeen & Tadhunter (1993) for a difference in the distribution of R between radio sources of Fanaroff & Riley (1974) (FR) type I and type II morphology. If this difference is confirmed, it would be consistent with the fact that lower radio-power objects (i.e. FR Is) are less affected by beaming (i.e. have a lower Lorentz factor characteristic for their jets), as discussed in Morganti et al. (1995a).

In an attempt to obtain high-resolution core flux-density measurements for a complete sample of radio sources and thereby improve the estimate of R, we have carried out observations using the high resolution provided by the Parkes–Tidbinbilla Interferometer (PTI, Norris et al. 1990). This instrument gives estimates of the core flux densities on scales of ~ 0.1 arcsec at 2.3 GHz. Throughout this paper, we will call radio core the radio component unresolved (or slightly resolved) on this scale. Our aim is to use these data to investigate possible differences in the distributions of R depending on the optical properties and/or radio morphologies of the sources.

2 THE SAMPLE

The sample studied has been selected from the Wall & Peacock (1985, hereafter WP85) sample of radio sources, which is complete down to a flux density of 2 Jy at 2.7 GHz. Our subsample was selected from the WP85 sample using the following criteria: declination $\delta < 10°$ and redshift $z < 0.7$. The final complete sample contains 88 objects (Tadhunter et al. 1993; di Serego et al. 1994). Based on the optical characteristics, the objects can be divided into 68 galaxies, 18 quasars and 2 BL Lacs. Twelve of the objects classified as radio galaxies show broad optical emission lines (BLRGs; Tadhunter et al., in preparation), and these sources will be considered separately in the discussion.

Previous radio observations for the objects in the sample were obtained by Morganti et al. (1993) with the Very Large Array (VLA) and the Australia Telescope Compact Array (ATCA) at 6 cm (with a resolution of about 3.5 arcsec). For the remaining sources, information has been collected from the literature.

All the information about the selection of the sample, new identifications as well as the available radio, optical and X-ray data can be found in Tadhunter et al. (1993), Morganti et al. (1993), di Serego Alighieri et al. (1994) and Siebert et al. (1996).

Throughout this paper we assume that $H_o = 50$ km s^{-1} Mpc^{-1} and $q_o = 0$.

3 PTI OBSERVATIONS AND DATA REDUCTION

With the PTI we have observed 77 of the 88 sources of the sample. Of the remaining objects, two were not observed because of constraints in our scheduled time, while for the other sources good high-resolution VLBI images were already available. The PTI gives real-time interference fringes over a single baseline of 275 km linking the Parkes Radio Telescope with one of the antennas at the NASA Deep Space Network Tracking Station at Tidbinbilla. The disadvantage of the PTI is that it cannot produce images but can only measure the correlated flux; the advantage is that observations are simple and data reduction is much faster than for VLBI observations.

The observations were done at 2.3 GHz and carried out in three observing runs during 1994 January, June and September (see Table 1 for the log of the observations). At the chosen frequency of 2.3 GHz, the PTI provides a resolution, λ/D, of about 0.1 arcsec that, for the redshifts of our sources, corresponds to at most 1 kpc. Apart from the 64-m antenna in Parkes, we used either one of the 34-m (mainly DSS45) or the 70-m antennas in Tidbinbilla, depending on availability. In column 3 of Table 1 are listed the antennas

Table 1. Log of the observations.

Session	Date	Antennas (m)
1	25/26-Jan-94	34-64
2	18-June-94	34-64
3	18-June-94	70-64
4	3/4-Sept-94	34-64
5	3/4-Sept-94	70-64

Table 2. PTI calibrators.

Name	Flux Jy	Session
PKS 0537−441	3.18	1
	4.37	4,5
PKS 1144−379	2.55	1
PKS 1921−293	12.7	2,3
	13.6	4

used in each session. The rms noise of a single 10-min integration is about 1.5–2.0 mJy for the observations with the 34-m antenna and ~0.8 mJy for those with the 70-m antenna.

The observations were divided in scans of about 10 min. For most of our objects we succeeded in having more than one scan (see below) taken at different hour angles. This is important both to test the reliability of the measured flux density and to see if any structure is present on a scale of 0.1 arcsec.

Flux-density calibrators were observed at the beginning and end of each observing session and their total flux was estimated from single-dish measurements made at the end of each session. This is an important requirement, given that many of the sources that can be used as PTI calibrators are variable. The list of calibrators used and their single-dish fluxes are given in Table 2. Variations in their flux density over the few months of our observations were clearly seen for both PKS 0537 − 441 and PKS 1921 − 293.

The individual observations for each source were analysed by looking at the average value of the visibility (as a function of time) and by Fourier transforming the complex correlation coefficients (see Slee et al. 1994 for more details). Slee et al. also discussed the errors associated with the flux-density measurements, finding a nominal error of the order of ~5 per cent. However, a larger source of uncertainty comes from either variability or structure in the sources partly resolved by the PTI. Slee et al. conclude that the combined effects of these factors result in an uncertainty of about 20 per cent in individual flux density measurements.

To quantify these uncertainties for our observations, we have compared the flux densities obtained for each object from the different scans. These scans are often separated by few hours in time in order to observe the source at different hour angles. However, for some sources, we have also repeated the observations in different observing runs, separated by months. In doing this we were always limited by the combination of scheduling constraints and observability of the sources. The distribution of the ratios of flux density obtained for every source in the different scans is shown in Fig. 1. The objects with a clearly resolved structure have been excluded from the plot. For some objects, in fact, modulations in their visibilities are visible during the 10-min scan, indicating that the source is resolved at the resolution of the PTI; these objects will be discussed in more detail in Section 4.2. The σ of the distribution indicates that an uncertainty of ~17 per cent affects the repeatability of our flux-density measurements. A further check on this uncertainty was made by comparing our new data and previous

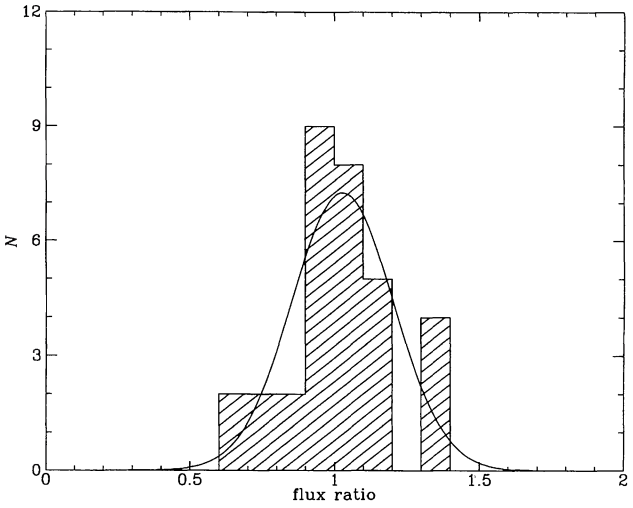

Figure 1. The distribution of the ratios of flux density obtained for every source in the different scans. The objects with a clearly resolved structure have been excluded from the plot. The solid line represents a Gaussian with σ of ~17 per cent.

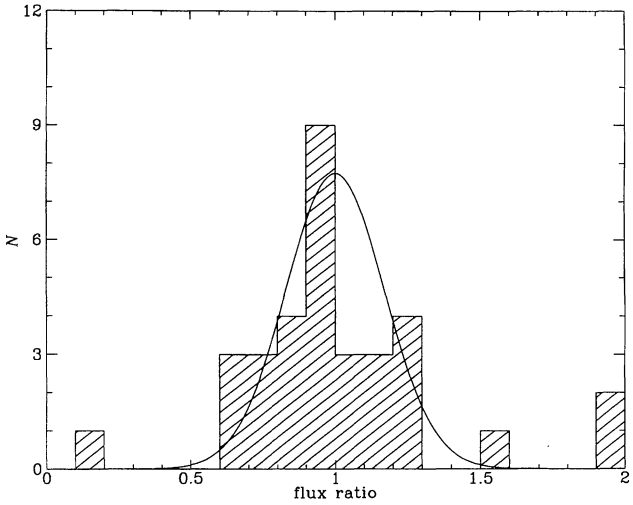

Figure 2. The distribution of the ratios between the flux density obtained from our observations and those obtained from the literature. The solid line represents a Gaussian with σ of ~17 per cent.

PTI observations available for some of the objects in the sample (Duncan et al. 1993; Slee et al. 1994; Jones, McAdam & Reynolds 1994). This comparison can tell us something more about uncertainty resulting from variability, given that these two observations are separated by years. Most of the objects in this comparison come from flat-spectrum objects (Duncan et al. 1993) where the variability should be stronger. The distribution of the ratio of these two flux-density measurements is shown in Fig. 2. In this figure we also overlay the Gaussian distribution obtained above.

Therefore, we conclude that our measurements have an uncertainty of up to ~17 per cent in which it is difficult to disentangle the effect of variability from structure in the source.

Table 3. Objects observed with the PTI.

Object	Other Name	z	Opt. type	Radio type	$S_{\rm core}^{2.3\rm GHz}$ Jy	$R_{2.3\rm GHz}$	$\log P_{\rm core}^{2.3\rm GHz}$ W Hz^{-1}	$\log P_{\rm tot}^{2.3\rm GHz}$ W Hz^{-1}	Notes
(1)	(2)	(3)	(4)	(5)	(6)	(7)	(8)	(9)	(10)
0023 − 26	OB-238	0.322	G	3	*	–	–	27.51	NLRG, CSS
0034 − 01	3C15	0.073	G	2	0.024	0.0095	23.77	25.80	WELG
0035 − 02	3C17	0.220	G	−1	0.411	0.1133	26.00	27.00	BLRG
0038 + 09	3C18	0.188	G	2	0.059	0.0200	25.04	26.74	BLRG
0039 − 44		0.346	G	−1	*	–	–	27.16	WELG
0043 − 42		0.116	G	2	0.0045	0.0009	23.46	26.51	NLRG
0045 − 25	NGC253	0.001	G	−1	0.014	0.0040	19.79	22.19	WELG
0055 − 01	3C29	0.045	G	1	0.055	0.0162	23.70	25.50	WELG
0105 − 16	3C32	0.400	G	2	<0.005	<0.0022	<24.72	27.37	NLRG
0117 − 15	3C38	0.565	G	2	<0.004	<0.0015	<24.94	27.77	NLRG
0123 − 01	3C40	0.018	G	1	0.079	0.0246	23.05	24.67	WELG
0159 − 11•	3C57	0.669	Q	2	0.713*	0.5540	27.31	27.76	
0213 − 13	3C62	0.147	G	2	0.0127	0.0046	24.12	26.47	NLRG
0252 − 71•		0.566	G	3	*	–	–	27.88	NLRG, CSS
0255 + 05	3C75	0.023	G	1	0.039	0.0120	22.96	24.89	WELG
0305 + 03	3C78	0.029	G	1	0.578	0.1214	24.33	25.30	WELG
0320 − 37	ForA	0.005	G	1	<0.004	$<4\times10^{-5}$	<20.64	25.03	WELG
0325 + 02	3C88	0.030	G	2	0.129	0.0423	23.71	25.11	WELG
0347 + 05		0.339	G	2	<0.0012[a],*	<0.0006	<23.78	27.01	BLRG
0349 − 27	OE-283	0.066	G	2	0.0105	0.0037	23.32	25.76	WELG
0403 − 13	OF-105	0.571	Q	4	0.68*	0.2753	27.00	27.66	
0404 + 03	3C105	0.089	G	2	0.019	0.0054	23.84	26.11	NLRG
0405 − 12•	OF-109	0.574	Q	2	0.8565*	0.5735	27.19	27.63	
0409 − 75		0.693	G	2	*	–	–	28.41	NLRG
0428 − 53		0.038	G	1	0.0638	0.0169	23.61	25.39	WELG
0442 − 28	OF-271	0.147	G	2	0.015	0.0039	24.21	26.62	NLRG
0453 − 20	OF-289	0.035	G	1	0.031	0.0112	23.23	25.18	WELG
0518 − 45	PicA	0.035	G	2	0.754*	0.0267	24.62	26.21	BLRG
0521 − 36		0.055	BL Lac	1	1.305*	0.1166	25.25	26.23	
0620 − 52•		0.051	G	1	0.123	0.0622	24.16	25.40	WELG
0625 − 35	OH-342	0.055	G	1	0.536	0.2267	24.86	25.59	WELG
0625 − 53		0.054	G	2	0.0285	0.0078	23.59	25.70	WELG
0637 − 75•		0.651	Q	4	4.31*	21.55	27.86	27.88	
0736 + 01•	OI61	0.191	Q	4	1.78	3.4231	26.47	26.58	
0806 − 10	3C195	0.110	G	2	0.0363	0.0148	24.32	26.15	NLRG
0842 − 75		0.524	Q	−1	0.133*	0.0659	26.35	27.56	
0859 − 25		0.305	G	2	<0.006	<0.0018	<24.52	27.26	NLRG
0915 − 11	HydA	0.054	G	1	0.157	0.0067	24.32	26.50	WELG
0945 + 07	3C227	0.086	G	2	0.012	0.0028	23.62	26.17	BLRG
1136 − 13	OM-161	0.554	Q	2	0.376	0.1551	26.85	27.72	
1151 − 34•	OM-386	0.258	Q	3	*	–	–	27.16	CSS
1246 − 41	NGC4696	0.009	G	−1	0.015	0.0068	21.73	23.90	WELG
1306 − 09	OP-10	0.464	G	3	*	–	–	27.54	NLRG, CSS
1318 − 43	NGC5090	0.011	G	1	0.411	0.1534	23.34	24.22	WELG
1333 − 33	IC4296	0.013	G	1	0.188	0.0190	23.15	24.87	WELG
1355 − 41		0.313	Q	2	0.096	0.0401	25.73	27.14	
1510 − 08•	OR-107	0.361	Q	−1	1.73	1.3622	26.98	27.22	
1514 − 24•	ApLib	0.048	BL Lac	−1	2.04	34	25.31	25.33	
1547 − 79		0.483	G	2	0.016	0.0071	25.37	27.53	BLRG
1549 − 79•		0.150	G	4	2.28*	1.3103	26.34	26.59	NLRG
1559 + 02	3C327	0.104	G	2	0.032	0.0064	24.22	26.42	NLRG
1602 + 01	3C327.1	0.462	G	2	0.078*	0.0378	26.05	27.49	BLRG
1648 + 05	HerA	0.154	G	1	0.009	0.0004	24.04	27.48	WELG
1717 − 00	3C353	0.031	G	2	0.078	0.0023	23.53	26.16	WELG
1733 − 56		0.098	G	2	0.468	0.0989	25.32	26.37	BLRG
1814 − 63		0.063	G	3	*	–	–	26.14	NLRG, CSS
1839 − 48•		0.112	G	1	0.129	0.0690	24.88	26.04	WELG
1932 − 46		0.231	G	2	0.015	0.0023	24.64	27.28	NLRG
1934 − 63•		0.183	G	3	12.15	–	27.31	27.28	NLRG, CSS
1938 − 15	OV-164	0.452	G	−1	*	–	–	27.68	BLRG
1949 + 02	3C403	0.059	G	2	0.024	0.0066	23.58	25.77	NLRG

Table 3 – *continued*

Object	Other Name	z	Opt. type	Radio type	$S_{\rm core}^{2.3\rm GHz}$ Jy	$R_{2.3\rm GHz}$	$\log P_{\rm core}^{2.3\rm GHz}$ W Hz^{-1}	$\log P_{\rm tot}^{2.3\rm GHz}$ W Hz^{-1}	Notes
(1)	(2)	(3)	(4)	(5)	(6)	(7)	(8)	(9)	(10)
1954 – 38•		0.630	Q	4	1.98	99	27.56	27.56	
1954 – 55		0.060	G	1	0.0433	0.0117	23.85	25.79	WELG
2058 – 28	OW-297.8	0.038	G	1	0.067	0.0221	23.64	25.30	WELG
2104 – 25	OX-208	0.037	G	2	0.0435	0.0060	23.43	25.65	WELG
2128 – 12•	OX-148	0.501	Q	4	1.9	19	27.34	27.36	
2135 – 14•	OX-158	0.200	Q	2	0.119	0.0633	25.37	26.60	
2135 – 20•	OX-20	0.635	G	3	*	–	–	27.80	BLRG,CSS
2152 – 69		0.027	G	1?	0.5825	0.0312	24.28	25.79	BLRG
2203 – 18	OY-106	0.618	Q	4	2.27	0.7747	27.67	28.03	
2211 – 17	3C444	0.153	G	2	<0.005	<0.0011	<23.79	26.74	NLRG
2221 – 02	3C445	0.057	G	2	0.09	0.0267	24.12	25.71	BLRG
2243 – 12•	OY-172	0.630	Q	4	2.61	20.077	27.73	27.45	
2250 – 41		0.310	G	2	<0.024[a],*	<0.001	<24.14	27.11	NLRG
2314 + 03•	3C459	0.220	G	2	0.667*	0.3940	26.24	26.78	NLRG
2345 – 16•		0.576	Q	–1	2.74*	2.0448	27.67	27.84	
2356 – 61		0.096	G	2	0.0205	0.0020	23.97	26.67	NLRG

*Resolved on the PTI observations (see Sejction 4.2).
[a]From VLA 5 GHz data, resolved on the PTI (see Section 4.2).
•Objects not included in the SSD sample.

4 RESULTS

In Table 3 we present the list of the sources observed with the PTI. Together with some of their radio and optical characteristics taken from the literature (see below), we list the measured core flux density, the core power from the PTI data (columns 6 and 8) and the total power from WP85. Some of the objects, marked in the table, appear to be resolved in our PTI data. These objects will be discussed in the next Section 4.2.

The radio classification, according to the scheme of Fanaroff & Riley (1974), is given in column 5 of Table 3 with FR I and FR II indicated as 1 and 2, respectively. To this we added compact steep spectrum (CSS, type 3), compact flat spectrum (CFS, $\alpha < 0.5$, type 4) and unclassified (type -1). This classification is mainly taken from Morganti et al. (1993), where the uncertainties of this classification are also discussed and, for a few objects, from Zirbel & Baum (1995) and Stickel, Meisenheimer & Kühr (1994). In a few cases, the morphological classification appears to be different in Morganti et al. and Zirbel & Baum, but this does not affect the results discussed below. The $R_{2.3\ \rm GHz}$ parameter (column 7) is defined as $R = S_{\rm core}/(S_{\rm tot} - S_{\rm core})$. Given that our core flux densities are at 2.3 GHz, we use the 2.7-GHz total power flux from WP85 to estimate R.

The optical classifications, given in column 4, are taken from Tadhunter et al. (1993). In addition, we give a further classification of the optical spectra (column 9) for the radio galaxies (using the data given in Tadhunter et al. (1993) and Tadhunter et al., in preparation). In particular we separate the galaxies into three groups: those with strong narrow emission lines (NLRGs), strong broad (FWHM > 2000 km s^{-1}) emission lines (BLRGs) and those with weak emission lines (WELG). The latter are identified by $\log L_{[\rm O\,III]} < 41.0$ erg s^{-1} together with stellar absorption lines or the 4000-Å break. Some of the galaxies classified as NLRGs in Tadhunter et al. (1993) are reclassified as BLRGs based on new data (Tadhunter et al., in preparation).

For completeness we list the radio and optical characteristics in Table 4 for the objects of the sample that were not observed with the PTI.

4.1 The PTI radio flux densities

Most of the data previously available on the core flux density of the objects come from ATCA/VLA observations and are presented in Morganti et al. (1993). Eleven objects had only an upper limit for their core flux density available from the previous ATCA/VLA observations. Among them we now find a marginal detection for the core of 0043 – 42, and we detect 0442 – 28, 1547 – 79 and 1932 – 46. The core of Fornax A (0320 – 37) was detected with the VLA and with the Molonglo Synthesis Radio Telescope (Fomalont et al. 1989; Jones & McAdam 1992) but it is undetected with the PTI. This non-detection at the resolution of PTI confirms the result already obtained by Slee et al. (1994) in previous PTI observations.

Fig. 3 shows the new PTI flux-density measurements plotted against the core flux densities derived from the ATCA/VLA maps. A strong correlation is visible between the two flux densities. However, we should point out that the frequencies of the two data sets are different as the ATCA/VLA observations were made at 5 GHz. The solid line represents a one-to-one correspondence between $S_{\rm PTI}^{2.3\ \rm GHz}$ and $S_{\rm ATCA/VLA}^{5.0\ \rm GHz}$: an offset between the ATCA/VLA and the PTI flux densities (with $S_{\rm PTI}^{2.3\ \rm GHz}$ systematically lower than $S_{\rm ATCA/VLA}^{5.0\ \rm GHz}$) is visible in the plot. The dashed line corresponds to the offset in the flux-density ratios at the two frequencies if a spectral index of $\alpha = -0.3$ ($S \propto \nu^{-\alpha}$) is considered. A value of -0.28 has been found for low-luminosity radio galaxies by Slee et al., while a spectral index of

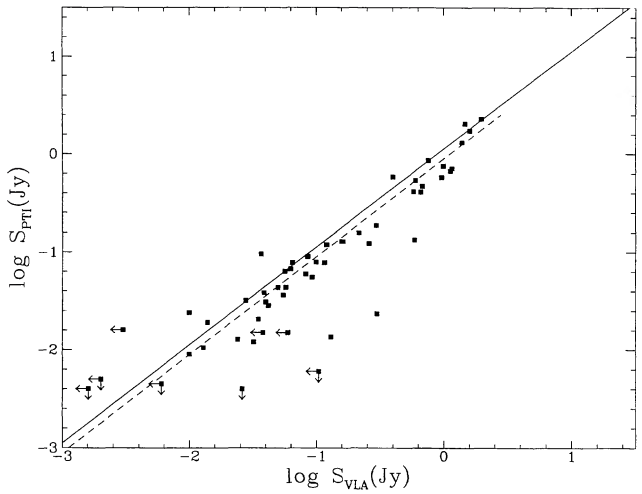

Figure 3. The new PTI flux densities plotted against the core flux densities derived from the ATCA/VLA maps. The solid line represents $S_{PTI}^{2.3\,GHz} = S_{ATCA/VLA}^{5.0\,GHz}$. The dashed line corresponds to the offset in the flux densities ratios at the two frequencies if a spectral index of $\alpha = -0.3$ ($S \propto \nu^{-\alpha}$) is considered.

-0.3 has been found for the overall radio emission from flat spectrum quasars (FSQs) by Padovani & Urry (1992). One can see from the figure that an inverted spectral index of -0.3 can, in fact, account for a large fraction of the offset. Therefore, such an inverted spectral index seems to be common to the wide range of objects represented in our sample. The remaining small offset (between the ATCA/VLA and PTI flux densities) is probably due to the different resolution of the observations.

If the spectral index is responsible for most of the difference in the measured flux densities, this means that even on the arcsecond scale the flux of the central region is dominated by a component with a much smaller scale (at least sub-arcsec). Over the redshift range of our sample, in fact, the linear scale in the ATCA/VLA observations ranges from ~ 1 kpc for the lower redshifts to ~ 30 kpc for $z = 0.7$, while for the new PTI observations the linear scale ranges from ~ 0.03 to ~ 1 kpc. As mentioned in the Introduction, this linear size of the PTI observations will correspond not only to the very nuclear region but will also include the base of the jet(s) (if present).

From Fig. 3 a larger scatter is also visible for the low-flux core (flux densities very close to the noise level) and for some other objects that deviate very clearly from the correlation. Among the radio galaxies, two objects have a very large radio between the ATCA/VLA and PTI data: the nearby starburst 0045 − 25 (NGC 253, ratio ~ 9) and 0034-01 (ratio ~ 12). For the latter, a high-resolution image will be necessary to explain this large discrepancy. Among the quasars, the largest ratio (~ 4.5) is observed in 0842 − 75.

For the objects listed in Table 4, i.e. with radio data taken from the literature and for which only the 5-GHz core flux density is available, we have converted it to 2.3 GHz, assuming the spectral index to be $\alpha = -0.3$.

4.2 Resolved objects

22 of the observed objects show modulations in the visibilities during the 10-min scan of the observations, thus indicating that structure is present. These objects are labelled in Table 3.

Using the time-scale of the modulations of the visibilities, one can, in principle, estimate the angular size of the compact structures that produce such modulations. We find two different groups of objects. In the first group, the actual period of the modulation is quite short ($\ll 10$ min) and the minimum of the modulation gets close to zero; these modulations are produced by structures on a large scale. This group includes 5 objects: 0039 − 44, 0347 + 05, 0409 − 75, 1938 − 15 and 2250 − 41. In all these cases, the compact structures are coincident with hot spots, arcseconds away from the nucleus. This is confirmed by looking at the low-resolution ATCA/VLA maps available. Thus, the PTI data cannot give any information about the core flux of these objects and in the analysis given below (as well as in Table 3) we use, if available, the value from the ATCA/VLA data (after correcting for the spectral index).

The second group includes 17 objects for which, because of the limited length of our scans (10 min), the exact period of the modulations can not be measured (i.e. the period is $\gg 10$ min). The long period and the fact that the modulations are only a small fraction of the peak flux, tell us that there must be structure on a small scale ($\ll 1$ arcsec). For most of these objects we are probably beginning to resolve the structure at the base of the jet. Nevertheless, we have included the flux densities for these objects in Table 3.

Table 4. Objects from the literature.

Object	Other Name	z	Opt. type	Radio type	$S_{core}^{2.3GHz}$ Jy	$R_{2.3GHz}$	$\log P_{core}^{2.3GHz}$ W Hz^{-1}	$\log P_{tot}^{2.3GHz}$ W Hz^{-1}	Notes
(1)	(2)	(3)	(4)	(5)	(6)	(7)	(8)	(9)	(10)
0131 − 36	NGC612	0.030	G	2	0.030	0.0054	23.08	25.35	WELG
0235 − 19	OD-159	0.620	G	2	$< 2 \times 10^{-4}$	$< 7 \times 10^{-5}$	<23.63	27.81	NLRG
0240 − 00	NGC1068	0.004	Seyf.	−1	0.059	0.019	21.62	23.34	
0430 + 05•	3C120	0.033	G	1	2.730	10.19	25.09	25.13	BLRG
1216 + 06	3C270	0.006	G	1	0.24	0.0194	22.58	24.30	WELG
1226 + 02	3C273	0.158	Q	−1	20.700	1.14	27.35	27.63	
1251 − 12	3C278	0.015	G	1	0.07	0.016	22.84	24.65	WELG
1253 − 05	3C279	0.538	Q	−1	9.15	4.46	27.97	28.06	
1322 − 43	CenA	0.002	G	1	5.51	0.045	22.89	24.26	WELG
1514 + 07•	3C317	0.048	G	1	0.31	0.163	24.24	25.09	WELG
1637 − 77		0.041	G	2	0.15	0.040	24.04	25.45	WELG

However, it should be noted that extra uncertainty could be associated with the number given in Table 3.

For some objects, we know that the slightly resolved structure may have nothing to do with the core. These are the (so-called) compact steep-spectrum (CSS; Fanti et al. 1995) sources of our sample. The CSSs are known to be very small sources that in most cases, on a VLBI scale, show a structure similar to the large-scale radio galaxies. The high-resolution VLBI maps available for the CSSs in our sample (King et al. 1996: Tzioumis et al. 1996) show, in fact, that they are typical double-lobed sources, scaled versions of the large radio galaxies. However, given their still uncertain position in the 'taxonomy' of the radio sources, they will not be discussed further here.

5 DISCUSSION

We will now use the new core flux densities, together with other radio and optical characteristics, to investigate if and how they are related to one another. The median values for z, $\log P_{\rm tot}$, $\log P_{\rm core}$ and $\log R$, for the different groups of objects, are summarized in Table 5 and discussed below.

Table 5. Medians for the full sample.

Full sample Groups	z	$\log P_{\rm tot}$ W Hz^{-1}	$\log P_{\rm core}$ W Hz^{-1}	$\log R$	N
FR I	0.035	25.30	23.70	−1.66	23
FR II, NLRG	0.153	26.71	24.18	−2.53	17
FR II, WELG	0.039	25.68	23.55	−2.16	8
BLRG	0.188	26.55	25.07	−1.57	13
SSQ	0.546	27.63	27.25	0.056	18
FSQ	0.618	27.66	27.56	+1.28	7

The nearby starburst NGC 253 and the Seyfert galaxy NGC 1068 have been excluded from the calculation of the medians.

5.1 Core powers and optical properties

Using the new flux densities of the cores estimated from the PTI data, we have constructed a $\log P_{\rm core}^{2.3\,\rm GHz}$ versus $\log P_{\rm tot}^{2.7\,\rm GHz}$ diagram. The plot is presented in Fig. 4, in which different symbols are used according to the different spectroscopic characteristics (regardless of their radio morphological classification) of the objects as described in Tables 3 and 4. This will allow us to investigate how the different spectroscopic characteristics of the host galaxies are distributed compared to the radio properties. A similar plot, but with the objects divided according to their radio morphology (and using only the ATCA/VLA data), has already been presented in Morganti et al. (1995a). In that paper it was argued that the overall shape of the plot cannot be explained as arising from selection effects related to the flux-density limit of the sample. Using Monte Carlo simulations, it has been shown that the diagram can be explained assuming that low-power sources are less affected by beaming because they have, on average, a lower Lorentz factor.

From their spectroscopic characteristics, we find that, as expected, the objects with weak emission lines (this includes mainly FR I but also some FR II objects; see Laing et al. 1994; Morganti et al. 1995b) also have the weakest total power. For total power larger than $\log P_{\rm tot} > 26.0$, we notice that *the galaxies with strong narrow emission lines represent, on average, the objects with relatively weaker cores, while the broad-line objects (radio galaxies and quasars) are the objects with relatively strong cores.* This was, of course, well known to be the case for quasars, but it is interesting to see that BLRGs also follow the same trend.

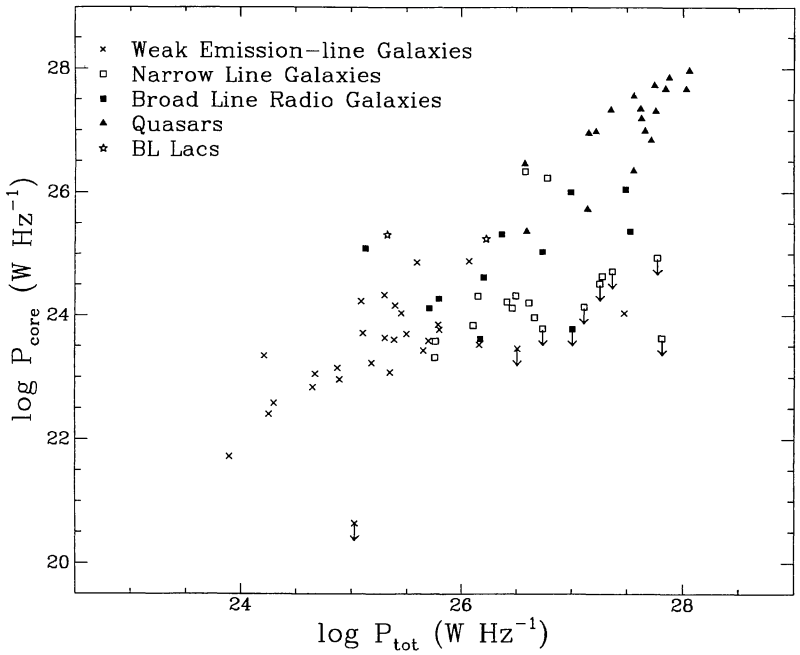

Figure 4. Plot of $\log P_{\rm core}^{2.3\,\rm GHz}$ versus $\log P_{\rm tot}^{2.7\,\rm GHz}$. The different symbols are used according to the different spectroscopic characteristics of the objects as described in Tables 3 and 4.

Few objects deviate from this trend; for them, a more detailed study of their radio and optical characteristics is necessary. Among the NLRGs, 1549−79 and 2314+03 have large relative core flux densities. The former is a compact radio source while the latter has a bluer optical continuum than normal galaxies and a radio structure very atypical for radio galaxies (Morganti et al. 1993). Among the WELG, Hercules A (1648+05) is the most striking exception, having a very high radio power for an object with very weak emission lines. On the other hand, this object is peculiar in many respects (see also the very high X-ray flux, Feigelson & Berg 1983; Siebert et al. 1996) and, at the moment, the reason for this it is not clear.

For WELGs, the median redshift (see Table 5) is more similar to that of FR I radio galaxies, i.e. much lower than the FR II, as is also the total power. This, together with the difficulties in their classification, seems to indicate that they are a transition group of radio galaxies, intermediate between FR I and II.

Given the difference in the redshift distribution of the different groups, a direct comparison of the core and total power can be misleading. A comparison using a sub-sample of objects will be done in Section 5.3.

5.2 Distribution of *R*

The results of the previous section can be seen even more clearly from the distributions of the radio core dominance R for the different groups of objects.

Based only on the radio classification (FR type), the distribution of $\log R$ appears to be clearly different for FR I and FR II radio galaxies (see Fig. 5 and Table 5). A probability $\ll 1$ per cent has been found, from the Kolmogorov–Smirnov (KS) test, for the two distributions deriving from the same population. A 'mild' difference between the two groups of objects has already been pointed out in Morganti et al. (1993), but now, with all the data available, this difference is clear, thus strengthening the results obtained in Morganti et al. (1995a) and summarized in Section 5.1. The two FR I objects that show a very low value of $\log R$ are 0320−37 (Fornax A) and 1648+05 (Hercules A), both mentioned above.

Let us now consider also the optical information for the radio galaxies. In Fig. 6 we present the distribution of $\log R$ for the FR II radio galaxies divided according to their optical characteristics. The median values of those distributions are given in Table 5. The NLRGs (these objects are all associated with FR II radio morphology) show the lower median value of R ($\log R = -2.52$, with 6 upper limits in R). The FR II–WELGs have a slightly higher value ($\log R = -2.16$), although this difference is not statistically significant, intermediate between the NLRGs and the FR I (which show a median $\log R = -1.66$).

The BLRGs show a distribution clearly different from that of the NLRGs, with a higher median value of R ($\log R = -1.57$). Moreover, only one upper limit to the core power has been found among the BLRGs (0347+05). From a KS test, we find a probability of ~ 0.4 per cent for the two distributions (BLRGs and NLRGs) deriving from the same population. We should also point out that the BLRGs include two objects classified as FRI (3C120 and 2152−69) although this classification (especially in the case of 2152−69) is very uncertain.

The larger value of R characteristic of BLRGs indicates that NLRGs and BLRGs also show different characteristics at radio wavelengths.

If we concentrate on the objects with strong emission lines, dividing the quasars into steep spectrum (SSQ, $\alpha > 0.5$) and flat spectrum (FSQ, $\alpha < 0.5$) (see Table 5), we find a continuity between the median value of R going from the NLRGs to the FSQs (Fig. 7). The latter show, as expected, the higher value of R ($\log R = 1.28$). The BLRGs fit well in the trend, with a value of R intermediate between NLRGs and SSQs. The distribution of BLRGs and SSQs appears to be significantly different (probability ~ 0.2 per cent for the two distributions deriving from the same population).

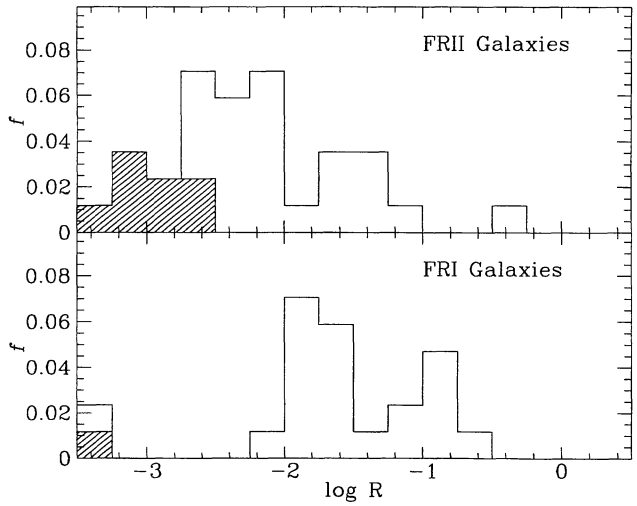

Figure 5. Distribution of $\log R$ for FR I and II radio galaxies. The y-axis represents the fraction of the sources normalized to the whole sample.

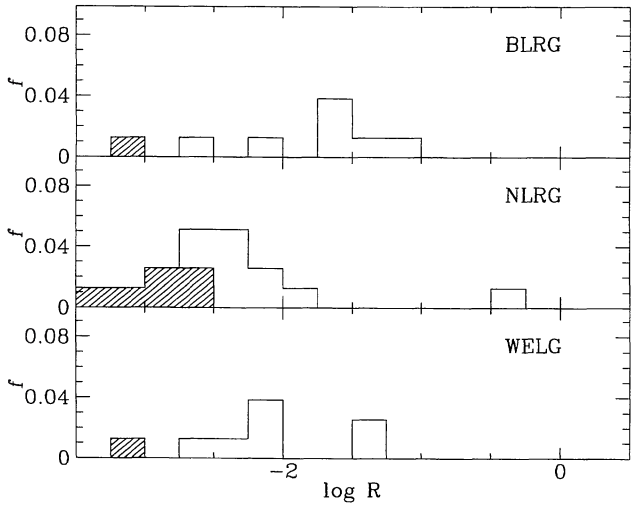

Figure 6. Distribution of $\log R$ for the FR II radio galaxies divided according to their optical characteristics. The y-axis represents the fraction of the sources normalized to the whole sample.

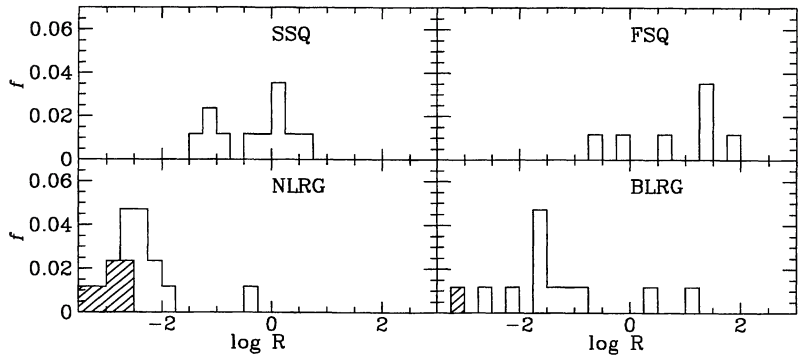

Figure 7. Distribution of $\log R$ for the radio galaxies and quasars with strong emission lines. The y-axis represents the fraction of the sources normalized to the whole sample.

We can interpret these results in the framework of the simpler 'unified scheme' (in which the AGN differ only by orientation and no difference in the molecular tori are taken into account). In this model, the SSQs and FSQs are believed to be increasingly aligned versions of FR II radio galaxies (in particular NLRGs). This implies increasingly strong beaming effects, which translate into a stronger core dominance. The closer alignment allows us to look further down into the nucleus (i.e. due to weaker effects of obscuration of the disc or torus around the active nucleus) and the broad emission lines are clearly observed (Barthel 1989; see also Urry & Padovani 1995 for a review). The situation for the BLRGs is more uncertain. They may either be objects intermediate between quasars and radio galaxies (i.e. with the nucleus only partly obscured and the broad emission lines just becoming visible at the edge of the obscuring torus), or they may represent the low-z, low-power equivalent of quasars.

From our observations we find that the BLRGs are more core-dominated than the NLRGs. A similar result, i.e. a trend between the value of R and the width of the optical emission lines, has been reported by Hine & Longair (1979) for a subsample of the 3CR sample of radio sources. This result agrees with the finding, from soft X-ray *ROSAT* observations (Siebert et al. 1996), that the BLRGs have a higher detection rate and, on average, a higher soft X-ray luminosity than the NLRGs. Therefore, we can confirm that the BLRGs are more similar to the quasars than are the NLRGs. However, the fact that the median of the R distribution for BLRGs is significantly lower than that of SSQs tends to support the idea that BLRGs are objects with an orientation (with respect to the line-of-sight) intermediate between NLRGs and QSRs. Moreover, it is interesting to note that the medians of the redshift distributions for the BLRGs (median $z=0.188$) and NLRGs (median $z=0.153$), in the complete sample, are quite similar.

On the other hand, this result does not seem to agree entirely with that found from a study of the X-ray spectral characteristics of the BLRG 3C390.3 (Inda et al. 1994). Its X-ray spectrum up to 30 KeV (from *Ginga* and *EXOSAT* data) can be described by a relatively flat, unabsorbed power law (with photon index Γ in the range of 1.5–1.8). This is quite similar to the typical spectral characteristics of SSQs rather than to radio galaxies, in which (in the few well-studied cases) obscuration produced by the nuclear torus is quite strong in the X-ray (see e.g. Cygnus A, Ueno et al. 1994). However, no definite conclusion can be drawn from just one object and more X-ray observations of BLRGs will be necessary.

5.3 Selection effects

The comparison between radio galaxies and quasars, based on the sample as a whole, can be influenced by strong selection effects. Because of the high selection frequency (2.7 GHz), our sample is biased in favour of strong, flat-spectrum core sources. This implies that the quasars in our sample are likely to have relatively stronger cores than quasars in samples selected at lower frequencies on the basis of extended steep-spectrum emission (e.g. 3C). This will affect the steep- as well as the flat-spectrum quasars. Thus, we have tested our results on a subsample [a so-called steep-spectrum-dominated (SSD) sample] selected on the basis of extended emission that is an *isotropically* emitted component. The sample is formed by the objects with $S^{\rm ext}_{2.7\,\rm GHz} > 2$ Jy. Many of the steep-spectrum, and all but two of the flat spectrum, quasars drop out of this sample. The median of the distribution for z, and the radio parameters of the different groups, are given in Table 6. The number of NLRGs and BLRGs does not change significantly from the SSD sample to the complete sample. It is therefore not surprising that the distribution of R for NLRGs and BLRGs is still significantly different. On the other hand, although the median $\log R$ for the SSQs decreases (median $\log R = -0.56$) and the number of objects becomes quite small, we still find the two distributions (BLRGs and SSQs) significantly different (probability ~ 1 per cent), see also Fig. 8.

While the R parameter is independent of redshift, a comparison of other parameters for different groups of objects is complicated by possible differences in the distributions of redshift, as appears evident from Table 5. Unlike radio galaxies, the distribution of z for SSQs and for FSQs peaks, as expected, at high z. To make the comparison between radio galaxies and quasars more balanced, we have restricted the redshift range to $z > 0.2$ and listed in Table 6 the medians of the distributions of $\log R$, $\log P_{\rm ext}$ and $\log P_{\rm core}$ for the different groups. Because the number of galaxies left is not very large, the statistic becomes more uncertain. In the case of NLRGs, all but one of the remaining objects have an upper limit for the core flux density: the median value reported in Table 6 is therefore quite uncer-

Table 6. Medians for the subsamples.

SSD sample Groups	z	$\log P_{tot}$ W Hz^{-1}	$\log P_{core}$ W Hz^{-1}	$\log R$	N
FR I	0.023	25.30	23.61	−1.72	19
FR II, NLRG	0.150	26.67	24.14	−2.64	16
FR II, WELG	0.039	25.68	23.55	−2.16	8
BLRG	0.188	26.56	24.83	−1.57	10
SSQ	0.538	27.66	27.00	−0.56	7
FSQ	0.595	27.85	27.34	−0.28	2
$z > 0.2$ sample Groups	z	$\log P_{ext}$ W Hz^{-1}	$\log P_{core}$ W Hz^{-1}	$\log R$	N
FR I	–	–	–	–	0
FR II, NLRG	0.355	27.28	(24.64)	(−2.75)	8
FR II, WELG	–	–	–	–	0
BLRG	0.457	27.24	26.00	−1.65	6
SSQ	0.571	27.34	27.31	+0.03	15
FSQ	0.595	27.48	27.62	+1.29	6

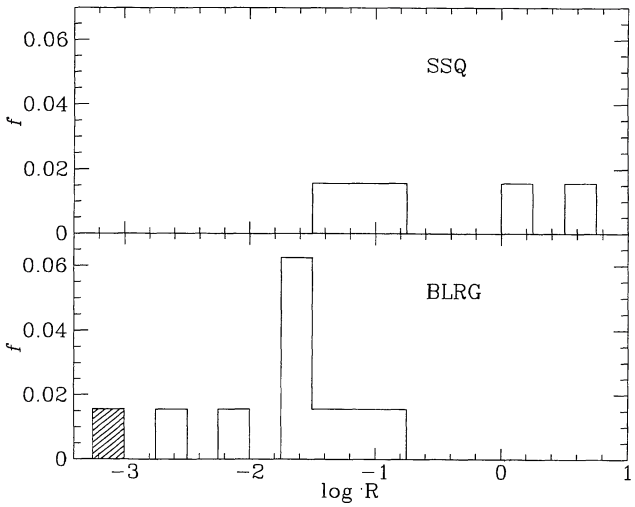

Figure 1. The distribution of the ratios of flux density obtained for every source in the different scans. The objects with a clearly resolved structure have been excluded from the plot. The solid line represents a Gaussian with σ of ~ 17 per cent.

tain. The distribution of R for BLRGs (median $\log R = -1.42$) appears to be still statistically different for SSQs. Also the core power of BLRGs appears to be intermediate between the NLRGs and the quasars. It is interesting to note that the distribution of the extended power is very similar in the different groups, suggesting that all sources have similar isotropic characteristics, as required by the unified schemes.

6 CONCLUSIONS

We have presented new radio flux density measurements for the cores in a complete sample of radio sources. These were obtained at 2.3 GHz with the Parkes–Tidbinbilla interferometer and correspond to a region between 0.03 and 1 kpc, for the redshift range of our sample.

The new data show that part of the difference between the old 5-GHz ATCA/VLA and the new 2.3-GHz PTI flux densities can be explained if an inverted spectral index of ~ -0.3 is taken into account. After considering the spectral index correction, we find that the measured flux densities do not change very much, going from a scale of tens of kpc (corresponding to the resolution of the previous ATCA/VLA observations) to the sub-kpc scale of the new observations. Thus, most of the flux observed in the central region originates in a sub-kpc area, likely combining the emission from the very compact central objects and the emission from the base of the (beamed?) jet(s).

The new data confirm the results already obtained in Morganti et al. (1995a) where, from the overall shape of the $\log P_{core}$ versus $\log P_{tot}$ plot and a 'mild' difference in the distribution of R for FR I and II radio galaxies, constraints on the value of the Lorentz factor were inferred for these sources. With the new data, the medians of the distributions of R for FR I and II appear to be statistically different, with FR I having a larger value of R. This has been explained as FR Is being less affected by beaming, because they have, on average, a lower Lorentz factor (Morganti et al. 1995a). Therefore, the core dominance R, in tests of unified schemes commonly used as an indicator of the orientation of a source, appears to depend also on the morphological classification.

On the other hand, combining the new core flux densities and the optical information on the sources in the sample, we found that *the radio core dominance shows different distributions for different optical characteristics*. The group of FR II with weak emission lines appears to have a value of R larger compared to the NLRGs and more similar to the FR I (as is median redshift). Again, among the FR II radio galaxies, NLRGs show the lower value of R while the BLRGs have a higher R, although it is still lower than that of the SSQs. This result is confirmed even if a number of selection effects are taken into account.

We have attempted to explain these results in the framework of the unified schemes for AGN. Our results are consistent with the idea that BLRGs have an orientation intermediate between NLRGs and SSQs. This result is also consistent with the finding obtained from the X-ray data (Siebert et al. 1996). The soft X-ray in the BLRGs is likely to be dominated by the contribution of the AGN. Moreover, Siebert et al. found a higher detection rate and, on average, a higher luminosity for BLRGs than for NLRGs. Because obscuration can be still significant in the soft X-ray, this can be considered as an indication of a more direct view of the active nucleus in the case of BLRGs compared to (e.g.) NLRGs.

ACKNOWLEDGMENTS

We are grateful to Dave Jauncey, whose useful suggestions and criticisms have helped in improving the manuscript.

REFERENCES

Barthel P. D., 1989, ApJ, 336, 606
di Serego Alighieri S., Danziger I. J., Morganti R., Tadhunter C. N., 1994, MNRAS, 269, 998
Duncan R. A., White G. L., Wark R., Reynolds J. E., Jauncey

D. L., Norris R. P., Taaffe L., Savage A., 1993, Publ. Astron. Soc. Austr., 10, 310
Fabbiano G., Miller L., Trinchieri G., Longair M., Elvis M., 1984, ApJ, 277, 115
Fanaroff B. L., Riley J. M., 1974, MNRAS, 167, 31P
Fanti C., Fanti R., Dallacasa D., Schilizzi R. T., Spencer R. E., Stanghellini C., 1995, A&A, 302, 317
Feigelson E. D., Berg C. J., 1983, ApJ, 269, 400
Fomalont E. B., Ebneter K. A., van Breugel W. J. M., Ekers R. E., 1989, ApJ, 346, L17
Hine R. G., Longair M. S., 1979, MNRAS, 188, 111
Inda M. et al., 1994, ApJ, 420, 143
Jones P. A., McAdam W. B., 1992, ApJS, 80, 137
Jones P. A., McAdam W. B., Reynolds J. E., 1994, MNRAS, 268, 602
King E. et al., 1996, in Ekers R. D. E., Fanti C., Padrielli L., eds, Proc. IAU Symp. 175, Extragalactic Radio Sources. p. 75
Laing R. A., 1994, in Bicknell G. V., Dopita M. A., Quinn P. J., eds, ASP Conf. Ser. 54, 1st Stromlo Symposium on the Physics of Active Galaxies. Astron. Soc. Pac., San Francisco, p. 227
Morganti R., Killeen N., Tadhunter C. N., 1993, MNRAS, 263, 1023
Morganti R., Oosterloo T. A., Fosbury R. A. E., Tadhunter C. N., 1995a, MNRAS, 274, 393
Morganti R., Tadhunter C. N., Fosbury R. A. E., Oosterloo T. A., Danziger I. J., di Serego Alighieri S., Siebert S., Brinkmann W., 1995b, Publ. Astron. Soc. Austr., 12, 3
Norris R. P., Allen D. A., Sramek R. A., Kesteven M. J., Troup E. R., 1990, ApJ, 359, 291
Orr M. J. L., Browne I. W. A., 1982, MNRAS, 200, 1067
Padovani P., Urry C. M., 1992, ApJ, 387, 449
Readhead A. C. S., 1993, in Davis R. J., Booth R. S., eds, Sub-arcsecond Radio Astronomy. Cambridge University Press, Cambridge, p. 173
Siebert J., Brinkmann W., Morganti R., Tadhunter C. N., Danziger I. J., Fosbury R. A. E., di Serego Alighieri S., 1996, MNRAS, 279, 1331
Slee O. B., Sadler E. M., Reynolds J. E., Ekers R. D., 1994, MNRAS, 269, 928
Stickel M., Meisenheimer K., Kühr H., 1994, A&AS, 105, 211
Tadhunter C., Morganti R., di Serego Alighieri S., Fosbury R. A. E., Danziger I. J., 1993, MNRAS, 263, 999
Tzioumis A. et al., 1996, in Ekers R. D. E., Fanti C., Padrielli L., eds, IAU Symp. 175, Extragalactic Radio Sources. p. 73
Ueno S., Koyama K., Nishada M., Yamauchi S., Ward M. J., 1994, ApJ, 431, L1
Urry C. M., Padovani P., 1995, PASP, 107, 803
Wall J. V., Peacock J. A., 1985, MNRAS, 216, 173 (WP85)
Wilkes B. J., 1994, in Bicknell G. V., Dopita M. A., Quinn P. J., eds, ASP Conf. Ser. 54, 1st Stromlo Symposium on the Physics of Active Galaxies. Astron. Soc. Pac., San Francisco, p. 41
Zirbel E. L., Baum S. A., 1995, ApJ, 448, 521